PHYSICAL REVIEW B **92**, 220415(R) (2015)

Spin waves in full-polarized state of Dzyaloshinskii-Moriya helimagnets: Small-angle neutron scattering study

S. V. Grigoriev,[1,2] A. S. Sukhanov,[1,2] E. V. Altynbaev,[1,2] S.-A. Siegfried,[3] A. Heinemann,[3] P. Kizhe,[1,4] and S. V. Maleyev[1]

[1]*Condensed Matter Department, Petersburg Nuclear Physics Institute, NRC "Kurchatov Institute", Gatchina, 188300 St. Petersburg, Russia*

[2]*Faculty of Physics, Saint Petersburg State University, Ulyanovskaya 1, 198504 St. Petersburg, Russia*

[3]*Zentrum für Material- und Küstenforschung GmbH, Helmholtz Zentrum Geesthacht, 21502 Geesthacht, Germany*

[4]*Faculty of Physics, Grad-Kitezh University, 100000 Grad-Kitezh, Russia*

(Received 3 August 2015; revised manuscript received 1 December 2015; published 21 December 2015)

We develop the technique to study the spin-wave dynamics of the full-polarized state of the Dzyaloshinskii-Moriya helimagnets by polarized small-angle neutron scattering. We have experimentally proven that the spin-waves dispersion in this state has the anisotropic form. We show that the neutron scattering image displays a circle with a certain radius which is centered at the momentum transfer corresponding to the helix wave vector in helimagnetic phase k_s, which is oriented along the applied magnetic field **H**. The radius of this circle is directly related to the spin-wave stiffness of this system. This scattering depends on the neutron polarization showing the one-handed nature of the spin waves in Dzyaloshinskii-Moriya helimagnets in the full-polarized phase. We show that the spin-wave stiffness A for MnSi helimagnet decreased twice as the temperature increases from zero to the critical temperature T_c.

DOI: 10.1103/PhysRevB.92.220415 PACS number(s): 75.30.Ds, 75.25.−j

The competition between the ferromagnetic exchange interaction and the antisymmetric Dzyaloshinskii-Moryia (DM) interaction leads to the appearance of the helical magnetic structure in the cubic B20-type compounds [1,2]. The ferromagnetic exchange interaction with the constant J and the DM interaction with the constant D stabilize the homochiral structure with the helix wave vector $k_s = D/J$. The constants J and D determine the energy landscape of the magnetic system and therefore its spin dynamics as well. The external magnetic field H_{C2} is needed to transform the helix into the ferromagnetic collinear full-polarized (FP) state. The difference in the energies $g\mu_B H_{C2}$ between the FP and helical states is shown to be equal to Ak_s^2, where $A = SJ$ is the spin-wave stiffness and S is the ordered spin [3,4]. The highly anisotropic spin-wave spectrum has been predicted for the DM helimagnets in [3,5,6] with the linear dispersion at $\mathbf{q} \parallel \mathbf{k}_s$ and the quadratic dispersion at $\mathbf{q} \perp \mathbf{k}_s$ for the long-wave excitations ($q < k_s$). Thus was shown that the helimagnon behaves like an antiferromagnetic magnon in the longitudinal direction, but like a ferromagnetic one in the transverse direction. Another remarkable feature of the helimagnon spectrum is its intrinsic multimode nature caused by periodic potential of the helical structure.

There were numerous attempts to study the spin-wave dynamics in MnSi, one of the best-known representatives of the DM helimagnets [7–11]. The first neutron experiments were performed in the FP on MnSi in the magnetic field above H_{C2}. These measurements revealed the individual magnetic excitation mode [7,8]. The inelastic scans with constant Q were summarized in a quadratic dispersion curve $\epsilon_q = Aq^2 + \Delta$ with the spin-wave stiffness constant equal to $A = 52 \pm 2$ meV Å^2 with the field along [111] direction of the crystal at $T = 5$ K [7]. The same set of the data could be used to estimate the temperature dependence of the spin-wave stiffness. The recent investigations of the spin waves in MnSi in the helimagnetic state ($H \ll H_{C2}$) demonstrated a rich variety of the anomalous excitation spectra [10]. The latest study of the MnSi using high-resolution inelastic neutron scattering allowed one to resolve the band structure of helimagnons [11]. It was shown that the whole set of the data at $T = 20$ K is well described with the spin-wave stiffness constant equal to $A = 48$ meV Å^2. Furthermore, the authors of [11] could estimate the temperature evolution of the spin-wave stiffness in the single magnetic-helix domain.

The peculiarities of the magnon spectrum in the helimagnets both above and below H_{C2} was described by Kataoka in [5]. Kataoka has additionally pointed out the differences of the spin-wave energy for the helical systems with the antisymmetric exchange interactions (DM type) and those with the symmetric exchange interactions (RKKY type). Moreover, the spin-wave energy in the case of the DM interaction for the fields above H_{C2} was explicitly given:

$$\epsilon_{\mathbf{q}} = A(\mathbf{q} - \mathbf{k}_s)^2 + (H - H_{C2}), \tag{1}$$

where $\mathbf{k}_s$ matches the orientation of the external magnetic field and equals D/J. The sign of the DM constant determines the direction of the helix wave vector k_s being parallel or antiparallel with respect to the direction of the field. The dispersion curve looks similar to the ferromagnetic one but has the three important features. First, the only minimum of the curve is shifted from the position $\mathbf{q} = 0$. Second, the sign of the DM constant determines the preferred direction of the propagation of the spin waves. Third, the spin-wave gap related to the magnetic field is shifted for the value $g\mu H_{C2}$. The FP state of the DM helimagnets is predicted to be the only known system with the excitations described by the asymmetrical dispersion relation. The triple axis spectroscopy (TAS) used for such studies suffers from the low-Q resolution, which is of the order of the helix wave vector k_s, and therefore cannot reveal the chiral anisotropy of the spin-wave spectrum.

To verify the main features of the dispersion relation Eq. (1) one can apply the neutron scattering method that was used to measure the spin-wave stiffness in the ferromagnets [12–16]. The essence of the method was proposed at the beginning of the 1960s, then it was supplanted by the triple-axis spectroscopy, and renovated in the 1980s using

the polarized neutron technique. In its latest version [12–14] the small-angle polarized neutron scattering was used in the so-called inclined geometry, when the magnetic field was applied to the ferromagnetic sample in the direction inclined for 45° to the incident neutron beam. The polarized neutrons are used in order to extract the scattering arising from the spin waves. In this case the energy-integrated neutron cross section contains a part which depends on neutron polarization and has a left-right asymmetry in the plane determined by directions of the field and the neutron beam. It can be analytically shown in the case of the ferromagnet that this neutron scattering is concentrated mostly within a narrow cone limited by the cutoff angle θ_C. This scattering can be interpreted as scattering of the heavy neutron particle on the light magnon quasiparticle. The maximal scattering angle θ_C is equal to the ratio of the two masses. In this Rapid Communication we show the possibility to measure the main magnetic dynamic parameter of the helical magnets with the DM interaction using small-angle polarized neutron scattering technique.

The method can be considered as a complimentary one for a measurement of spin-wave stiffness constant by the triple axis spectroscopy. The main advantage of application of small-angle neutron scattering (SANS) is very high resolution of the SANS instruments in the Q space, which is orders of magnitude better than that of the TAS instruments. It is a key point for the system with DM interaction as the value of the helix wave vector k_s is very small. Thus, one cannot resolve the shifted position of the minimum of the spin-wave spectrum by means of TAS. The resolution in the momentum transfer of TAS is too rough to distinguish the dispersion curve so close to k_s. The small-angle neutron scattering technique can be applied in order to overcome this difficulty. Second the SANS method is much faster in the data collection to reach the statistic needed to satisfactorily treat the data. It is related to the integration over the energy transfer upon detection of the scattered neutrons. The method gains an additional factor as it works in the range of small angles where the magnetic form factor is close to 1. As a consequence, one can use a smaller amount of the sample for measurements, or make a much shorter exposition time. The disadvantage of the method is that it is model dependent. Nevertheless, if the model suits the system, as in the case of the DM ferromagnets, then it produces nice results.

Since the cross section is a scalar quantity, it may depend on the axial vector of polarization $\mathbf{P}_0$ of the incident beam only if the system is characterized itself by another axial vector. One of the most interesting examples of the axial-vector interaction—the Dzyaloshinskii-Moriya interaction—provides the polarization-dependent (chiral) scattering in the cubic helimagnets. As it was shown by Maleyev [17–19], the inelastic magnetic chiral contribution in the neutron cross section $\sigma_{\rm ch}(\mathbf{Q},\omega)$ can be represented by

$$\sigma_{\rm ch}(\mathbf{Q},\omega) = \frac{k_f}{k_i} 2r^2 |F_m|^2 \frac{1}{\pi(1-e^{-\omega/T})} \langle S\rangle P_0 (\hat{\mathbf{Q}}\hat{\mathbf{h}})^2 \times [\delta(\omega-\epsilon_{\mathbf{Q}}) + \delta(\omega+\epsilon_{-\mathbf{Q}})], \quad (2)$$

where k_f and k_i are momenta of the scattered and incident neutron, respectively, r is the classical electron radius, F_m is the magnetic form factor, $\langle S\rangle$ is the average atomic spin, and $\hat{\mathbf{Q}}$ is the unit vector along the momentum transfer. This equation takes into account that the initial polarization is directed along the unit vector of an applied magnetic field: $\mathbf{P}_0 = P_0\hat{\mathbf{h}}$, $\hat{\mathbf{h}} = \mathbf{H}/H$; $\epsilon_{\mathbf{q}}$ represents the spin-wave dispersion. Equation (2) is applicable for the cubic or amorphous ferromagnets with the conventional quadratic dispersion as well as for the field-induced ferromagnetic state of the cubic helimagnets with the dispersion relation given by Eq. (1).

In order to consider the kinematics of the small-angle scattering we introduce a Cartesian coordinate system with the z axis directed along the incident beam and the x axis along the magnetic field applied perpendicular to the incident beam. In the small-angle scattering approximation the momentum transfer $\mathbf{Q}$ can be split into the two elastic components, which are perpendicular to the vector of the incident neutron $\mathbf{k}_i$: $Q_x = k_i\theta_x$, $Q_y = k_i\theta_y$ with scattered angles along and perpendicular to the magnetic field respectively, and the inelastic z component, which is oriented along $\mathbf{k}_i$: $Q_z = k_i(\omega/2E_i)$, where E_i is the energy of the incident neutron. Thus we have for the length of the momentum transfer

$$Q = k_i\left[\theta_x^2 + \theta_y^2 + (\omega/2E_i)^2\right]^{1/2}. \quad (3)$$

If the energy transfer is small $\omega \ll T$, then one can replace $[1-\exp(-\omega/T)]^{-1}$ in Eq. (2) for T/ω. In the case of small-angle neutron scattering Eq. (2) has to be averaged over ω. Using Eq. (3) one can obtain the chiral contribution to the cross section as a function of the scattered angle θ:

$$\sigma_{\rm ch}(\theta) \sim \langle S\rangle T P_0 \int \frac{d\omega}{\omega} \frac{(2E_i\theta_x)^2}{\omega^2 + (2E_i)^2(\theta_x^2+\theta_y^2)} \times [\delta(\omega-\epsilon_{\mathbf{Q}}) + \delta(\omega+\epsilon_{-\mathbf{Q}})]. \quad (4)$$

According to the dispersion relation [Eq. (1)], the expressions in the δ functions of Eq. (4) have the form

$$\omega - \epsilon_{\mathbf{Q}} = \omega - Ak_i^2\left[\theta_x^2 + \theta_y^2 + \left(\frac{\omega}{2E_i}\right)^2\right] + 2Ak_i\theta_x k_s - H, \quad (5)$$

$$\omega + \epsilon_{-\mathbf{Q}} = \omega + Ak_i^2\left[\theta_x^2 + \theta_y^2 + \left(\frac{\omega}{2E_i}\right)^2\right] + 2Ak_i\theta_x k_s + H. \quad (6)$$

Using the standard transformation one can get

$$\delta(\omega-\epsilon_{\mathbf{Q}}) + \delta(\omega+\epsilon_{-\mathbf{Q}}) = \frac{\delta(\omega-\omega_1)+\delta(\omega-\omega_2)}{|1-\omega/(2E_i\theta_0)|} + \frac{\delta(\omega-\omega_3)+\delta(\omega-\omega_4)}{|1+\omega/(2E_i\theta_0)|}, \quad (7)$$

with the roots $\omega_i(\theta_x,\theta_y)$ of the quadratic functions in the right-hand sides of Eqs. (5) and (6):

$$\frac{\omega_{1,2}}{2E_i} = \theta_0 \pm \sqrt{\theta_C^2 - (\theta_x-\theta_B)^2 - \theta_y^2},$$
$$\frac{\omega_{3,4}}{2E_i} = -\theta_0 \pm \sqrt{\theta_C^2 - (\theta_x+\theta_B)^2 - \theta_y^2}, \quad (8)$$

where we introduce a dimensionless parameter $\theta_0 = (2Am_n)^{-1}$, which relates the spin-wave stiffness to the neutron

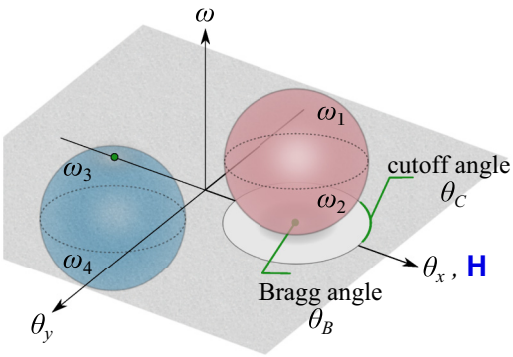

FIG. 1. (Color online) Roots of right-handed sides of Eqs. (5) and (6) ω_{1-4} as a function of the scattered angles θ_x,θ_y. Gray plane is $\omega = 0$ plane. The red sphere ($\omega_{1,2}$) placed in positive range of energy transfer, while the blue sphere ($\omega_{3,4}$) is located in negative range of ω.

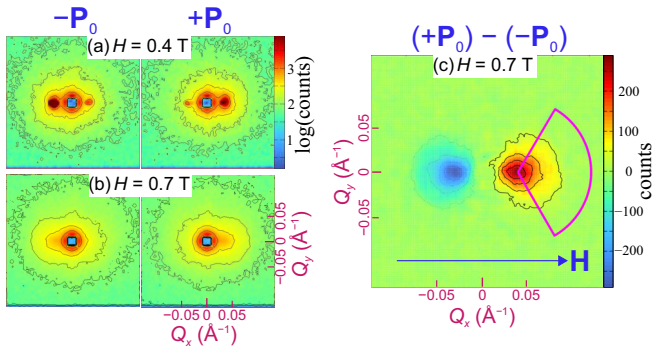

FIG. 2. (Color online) Maps of the SANS intensities for the chiral single crystal MnSi at $T = 15$ K at the field below H_{C2} (0.4 T) (a) and above H_{C2} (0.7 T) (b) for the polarization $\mathbf{P}_0$ opposite the guide field (left column) and along it (right column). (c) The result of the subtraction of the left and right SANS patterns at $H = 0.7$ T. The arrow shows a direction of the field.

mass m_n, and the angle θ_C:

$$\theta_C^2(H) = \theta_0^2 - \frac{\theta_0}{E_i} H + \theta_B^2. \tag{9}$$

A schematic view of the solutions given by Eq. (8) is presented in Fig. 1. As one can see, the roots $\omega_{1,2} \neq -\omega_{3,4}$, therefore, the integral of the antisymmetric function in Eq. (4) is nonzero. Two pairs of surfaces ($\omega_{1,2}$ and $\omega_{3,4}$) form two spheres in the (ω,θ_x,θ_y) space. If the incident neutrons is polarized along the magnetic field ($+\mathbf{P}_0$), then the scattering with the energy gain is only allowed, while the energy loss process is forbidden. A flip of the polarization $-\mathbf{P}_0$, on the contrary, allows scattering with the magnon annihilation process and makes the magnon creation process forbidden. The sign of the DM constant in this case determines whether the neutrons with $+\mathbf{P}_0$ will be scattered in the direction of the magnetic field (see Fig. 1, for example) or in the opposite direction.

As a consequence, the chiral scattering from the spin waves appears within the circle which has the radius given by θ_C in Eq. (9) and centered at the Bragg angle θ_B. Hence, θ_C is the cutoff angle for this type of scattering and bears the information about the spin-wave stiffness A. The cutoff angle depends also on the applied magnetic field and its square decreases linearly when the field increases. The observation of this scattering allows one to reveal the main features of the spin waves in the FP state of the DM helimagnets. Moreover, Eq. (9) provides a possibility to clearly extract the stiffness A from the measurement of the cutoff angle in the small-angle polarized neutron scattering experiment.

On the contrary for the ferromagnets with isotropic dispersion relation, the integral in Eq. (4) vanishes in the geometry with the magnetic field applied perpendicular to the incident beam. In order to provide the nonzero chiral scattering in the conventional ferromagnets, the magnetic field has to be inclined with respect to the direction of $\mathbf{k}_i$ [12–14].

The polarized small-angle neutron scattering (PSANS) were performed using the SANS-1 instrument at the FRM-II (Germany). A polarized neutron beam with initial polarization $P_0 = 0.93$ and mean wavelength $\lambda = 0.55$ nm was used. A magnetic field (0.1–1.5 T) was applied along Q_x. The MnSi single crystal, used in the experiment, is known to show a left-handed crystallographic configuration and also a left-handed spin helix [20]. Figure 2(a) shows a typical SANS map from the MnSi sample at the temperature below T_c and in the field H below H_{C2} with initial polarization opposite to $-\mathbf{P}_0$ and along $+\mathbf{P}_0$ the magnetic field. One can see the Bragg peaks at $\mathbf{Q} = \pm\mathbf{k}_s$ for the polarization along and opposite the field $\pm\mathbf{P}_0$. It is caused by the neutron scattering on the stable left-handed helix structure. The analysis of the diffuse scattering at $H < H_{C2}$ [Fig. 2(a)] is out of the scope of this paper.

As the field reaches the value of H_{C2}, the elastic scattering disappears completely and only the inelastic diffuse scattering centered at $\mathbf{Q} = \pm\mathbf{k}_s$ remains [Fig. 2(b)]. This scattering is well described by Eq. (4) and consists of the strong diffuse scattering in the vicinity of the former Bragg peak and a round spot limited by the critical angle θ_C. The diffuse scattering at $\mathbf{Q} = \pm\mathbf{k}_s$ is maximal at $H \sim H_{C2}$ and strongly suppressed by an increase of the field. The round spot centered at $\mathbf{Q} = \pm\mathbf{k}_s$ can be observed in the field range up to $H \approx 2H_{C2}$.

In order to extract the polarization-dependent scattering the patterns with the polarizations along and opposite to the magnetic field were subtracted one from another [Fig. 2(c)]. The presence of this chiral scattering confirms that the dispersion curve in the FP state of the DM helimagnets has the only minimum that is shifted at $\mathbf{q} = \mathbf{k}_s$.

To improve the statistics, the scattering intensity was radially averaged over the angular sector of 120° degrees with the center positioned at $\mathbf{Q} = \pm\mathbf{k}_s$ as shown in Fig. 2(c). The intensity is plotted as a function of the angle $\theta - \theta_B$ in Figs. 3(a)–3(d) at different values of the field and $T = 15$ K. The cutoff angle $\theta_C(H)$ can be easily obtained from the analysis of the I versus $\theta - \theta_B$ plot. The steplike edge of the measured intensity was fitted by the following function: $1/2 - (1/\pi)\arctan[2(\theta - \theta_c)/\delta]$. The position of the cutoff angle was determined as a center of the arctan function θ_C. Its width δ is related to the spin-wave damping.

Thus extracted values of the cutoff angle θ_C were plotted as a function of the field in Fig. 3(e) for $T = 15$ K. The square of the cutoff angle depends linearly on the field in accord with Eq. (9). Using Eq. (9) one can determine the value of the parameter θ_0 (and the spin-wave stiffness) with high accuracy.

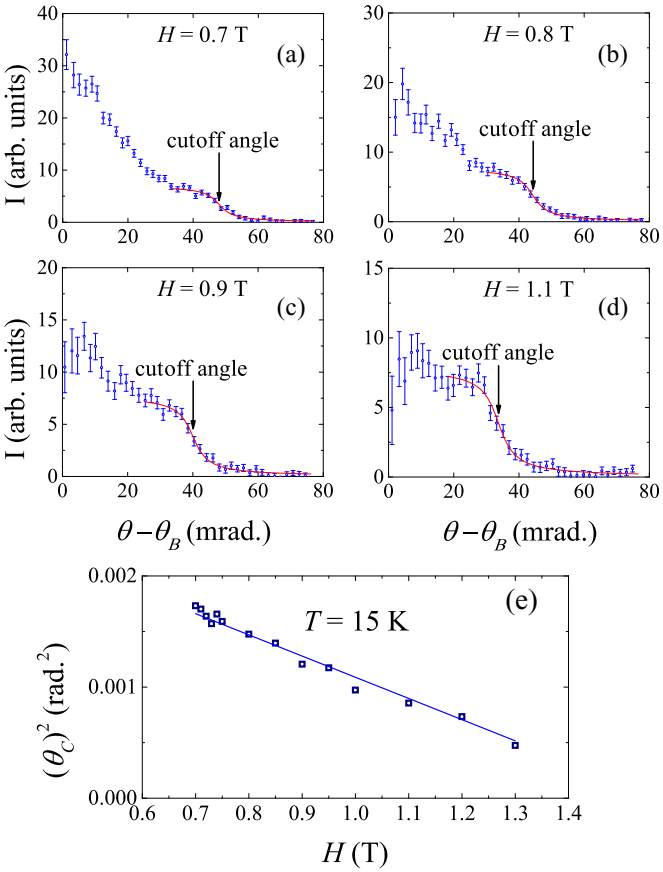

FIG. 3. (Color online) The radially averaged scattering intensity centered at the Bragg peak position I vs scattered angle $\theta - \theta_B$ at $H = 0.7$ T (a), $H = 0.8$ T (b), $H = 0.9$ T (c), $H = 1.1$ T (d). The solid lines near the steplike edge show the results of the best fits by the steplike function. The cutoff angle is observed. (e) The field dependence of the square of the cutoff angle θ_C^2 at $T = 15$ K. Error bars, obtained from the fit, are of the size of the symbols. The solid line is a linear fit by Eq. (9).

It is important to note that the Stoner continuum in MnSi takes places at a momentum transfer much larger than that considered in the present work. As was shown in [7], the spin-wave stiffness is field independent in the wide range of the applied field. Moreover, the effect of the field on stiffness would distort the linear law in the field dependence of the square of the cutoff angle.

The spin-wave stiffness, obtained from the detection of the cutoff angles at different temperatures is presented in Fig. 4. For completeness we added the points measured by the triple-axis spectroscopy in [7,9]. The value at 5 K given in [7] coincides with our results. The measured temperature dependence was fitted by the power law as follows: $A(T) = A_0[1 - c(T/T_C)^z]$, where z is equal to 1.8 ± 0.3 with $A_0 = 0.054$ meV Å^2 and $c = 0.47$.

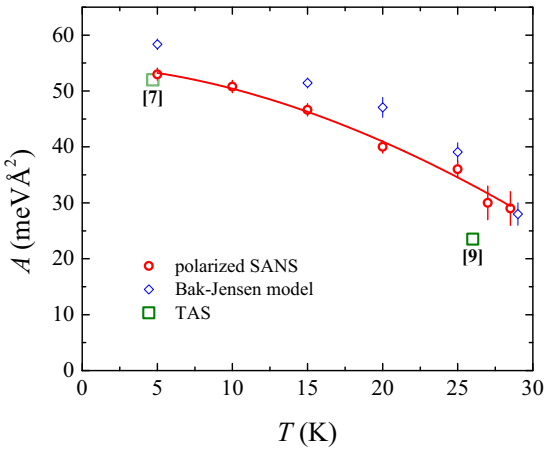

FIG. 4. (Color online) Temperature dependence of the spin-wave stiffness $A(T)$: circles—polarized SANS; squares—TAS [7,9], diamonds estimation from the Bak-Jensen model [3,4]. Solid lines are the fit by the power law (see text).

The spin-wave stiffness can be estimated from the theory by Bak and Jensen [3,4] using the ratio relating the critical magnetic field H_{C2} and the difference in the energies between the FP and helical states $g\mu_B H_{C2} = Ak_s^2$. The temperature dependence of the stiffness calculated in this model is shown in Fig. 4. Both the magnitudes of the stiffness and a trend for its small decrease with temperature are the same for the calculated and measured values, except a small discrepancy in the low-temperature range. The calculated values may be overestimated since the above-given expression should be slightly corrected by accounting for the cubic anisotropy [21]. Nevertheless, we show that the expression linking H_{C2} and k_s can be used for estimation of the spin-wave stiffness in the whole temperature range from zero to the critical temperature T_c.

In conclusion, we have experimentally proven the validity of the spin-wave dispersion relation for helimagnets with the DM interaction in the full-polarized state [Eq. (1)]. In spite of similarity with the ferromagnetic dispersion, it shows the only minimum that is shifted along the field axis from the position $\mathbf{q} = 0$ to the value of $\mathbf{k}_s$. Using polarized neutrons we demonstrate that the sign of the DM constant determines the preferable clockwise or anticlockwise rotation of the spin waves, i.e., the chirality of the DM helimagnets results in the one-handed excitations in the full-polarized state above H_{C2}. Analysis of the scattering allowed us to measure the temperature dependence of the spin-wave stiffness. This method can be used to investigate the parameter of the spin-wave dynamics in the other representatives of DM helimagnets.

The work was supported by the Russian Foundation for Basic Research (Grant No. 14-22-01073 ofi-m).

[1] O. Nakanishia, A. Yanase, A. Hasegawa, and M. Kataoka, Solid State Commun. **35**, 995 (1980).

[2] P. Bak and M. H. Jensen, J. Phys. C **13**, L881 (1980).

[3] S. V. Maleyev, Phys. Rev. B **73**, 174402 (2006).

[4] A. N. Bogdanov, U. K. Roessler, and C. Pfleiderer, Physica B **359-361**, 1162 (2005).

[5] M. Kataoka, J. Phys. Soc. Jpn. **56**, 3635 (1987).
[6] D. Belitz, T. R. Kirkpatrick, and A. Rosch, Phys. Rev. B **73**, 054431 (2006).
[7] Y. Ishikawa, G. Shirane, J. A. Tarvin, and M. Kohgi, Phys. Rev. B **16**, 4956 (1977).
[8] J. A. Tarvin, G. Shirane, Y. Endoh, and Y. Ishikawa, Phys. Rev. B **18**, 4815 (1978).
[9] F. Semadeni, P. Boni, Y. Endoh, B. Roessli, and G. Shirane, Physica B **267-268**, 248 (1999).
[10] M. Janoschek, F. Bernlochner, S. Dunsiger, C. Pfleiderer, P. Boni, B. Roessli, P. Link, and A. Rosch, Phys. Rev. B **81**, 214436 (2010).
[11] M. Kugler, G. Brandl, J. Waizner, M. Janoschek, R. Georgii, A. Bauer, K. Seemann, A. Rosch, C. Pfleiderer, P. Boni, and M. Garst, Phys. Rev. Lett. **115**, 097203 (2015).
[12] A. I. Okorokov, V. V. Runov, B. P. Toperverg, A. D. Tretyakov, E. I. Maltsev, I. M. Puzeii, and V. E. Mikhailova, Pis'ma v ZhETF **43**, 390 (1986) [JETP Lett. **43**, 503 (1986)].
[13] V. Deriglazov, A. Okorokov, V. Runov, B. Toperverg, R. Kampmann, H. Eckerlebe, W. Schmidt, and W. Lobner, Physica B **180-181**, 262 (1992).
[14] B. P. Toperverg, V. V. Deriglazov, and V. E. Mikhailova, Physica B **183**, 326 (1993).
[15] S. V. Grigoriev, S. V. Maleyev, V. V. Deriglazov, A. I. Okorokov, N. H. van Dijk, E. Bruck, J. C. P. Klaasse, H. Eckerlebe, and G. Kozik, Appl. Phys. A **74**, s719 (2002).
[16] S. V. Grigoriev, E. V. Altynbayev, H. Eckerlebe, and A. I. Okorokov, J. Surf. Invest.: X-Ray, Synchrotron Neutron Tech. **8**, 1027 (2014).
[17] S. V. Maleyev, Physica B **297**, 67 (2001).
[18] S. V. Maleyev, Phys. Usp. **45**, 569 (2002).
[19] S. V. Maleyev, Physica B **345**, 119 (2004).
[20] S. V. Grigoriev, D. Chernyshov, V. A. Dyadkin, V. Dmitriev, S. V. Maleyev, E. V. Moskvin, D. Menzel, J. Schoenes, and H. Eckerlebe, Phys. Rev. Lett. **102**, 037204 (2009).
[21] S. V. Grigoriev, A. S. Sukhanov, and S. V. Maleyev, Phys. Rev. B **91**, 224429 (2015).